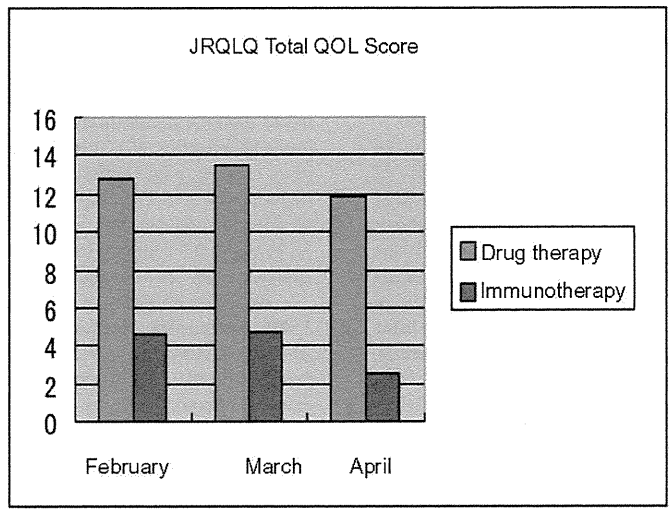

Fig. 3. **QOL scores in drug therapy and allergen immunotherapy for cedar pollinosis**

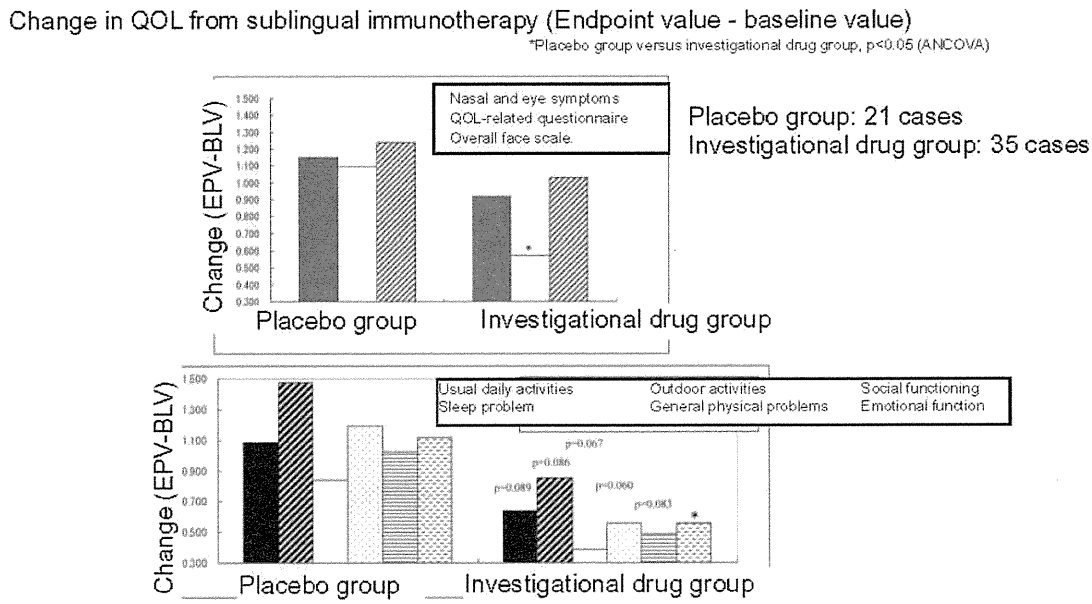

Fig. 4. **Change in QOL from sublingual immunotherapy (from Reference 22)**

as ineffective and even guidelines do not address this modality as a standard therapy. Outside Japan however, efficacy is reported. In pediatrics, there is a high level of evidence for efficacy in both bronchial asthma and allergic rhinitis [20]. There are also data showing that SCIT inhibits onset of asthma in pediatric pollinosis [21]. However, children reportedly have a higher incidence of anaphylactoid exaggerated immune response than adults, and care is required.

Sublingual allergen immunotherapy

After receiving Ethics Review Board approval for sublingual immunotherapy (SLIT) for cedar pollinosis as currently practiced in the EU and US, we began such practice in 1999 [22].

When administration is initiated, the concentration of antigen extracts is set at 2 JAU/ml, and concentration is increased daily in stepwise fashion until a maintenance level of 2000 JAU/ml is reached. Administration is performed by adding 1 to 20 drops (approximately 50 μL to 1 ml) of the prepared extract to a small piece of bread (roughly a 1.5 cm square), placing this

under the tongue for 2 minutes, and then removing the bread. Maintenance is provided as 20 drops of 2000 JAU/ml antigen extract administered sublingually 1×/week. Though the literature provides detailed results, deterioration of QOL was found to have been reduced to half that associated with placebo (***Fig. 4***)[22,23].

Progress in immunological research and associated technologies has already established alternative paths of immunotherapy in the EU, where it is widely used clinically. The methodology of treatment based on the hygiene hypothesis is also becoming better established, and its association with age should also be considered. Theoretically, combination of antigens and adjuvants in particular may come to represent the optimal treatment for allergic diseases. These therapeutic modalities may in the future be used to cure a number of allergic diseases, and primarily pollinosis, without regard to age. But at present, clinical use among humans remains low, and considerable study is required.

3) Herpes zoster and preventive vaccination for Herpes zoster

After a pediatric outbreak of varicella infection, the Varicella zoster virus (VZV) lies dormant in a ganglion and can cause shingles when triggered by stress or some other impetus. Shingles is an age-related disease. Among 48,388 shingles patients in Miyazaki Prefecture, the incidence of onset was 4.15/1000 persons annually, with the rate of onset increasing to 5-8/1000 persons at age 50 years or older, and by age 80 years, approximately 40% had experienced shingles (***Fig. 5***). Shingles has also increased in other reports, and Miyazaki Prefecture also saw an increase greater than 20% in these 10 years, with a notable increase among females age 60 years and older[24].

Herpes zoster is caused by the reactivation of a dormant virus in the trigeminal ganglia, dorsal root ganglia, or other afferent ganglion and migrates to the skin, damaging nerve bundles in the process. At such time, the pain associated with nerve damage is distinctive. In 75% of cases, prodromal pain proceeds eruption of a shingles rash by 3-5 days, and at age 50 years or older, pain continues even after healing of eruptions in a majority of cases. Postherpetic neuralgia (PHN) occurs in 9-19% of shingles patients, at a low risk of 2% in those less than age 50 years, at 20% among those greater than age 50 years, and at approximately 35% among those greater than age 80 years[25].

Based on 15 years of Herpes zoster epidemiology among 3500 community residents, Hope-Simpson observed that shingles declines when varicella is prevalent[26]. A subsequent report stated that shingles was infrequent among adults exposed occupationally to varicella patients. In the US state of Massachusetts, the incidence of varicella was reduced by 79%, from 16.5/1000person-years to 3.5/1000, over the period of 1998 to 2003 by introduction of routine vaccination with the live Oka varicella vaccine, but the incidence of herpes zoster increased by 90%, from 2.77/1000 to 5.25/1000[27]. This finding suggests that exposure to varicella can boost varicella immunity and prevent herpes zoster. Conversely, the absence of epidemic varicella was found to increase the incidence of herpes zoster in a cohort in which opportunities for immunoboosting were reduced.

On this basis, Oka varicella vaccine was used to prevent varicella, and attempts were made to boost immunity to the VZV and prevent shingles by inoculating adults and elderly individuals with Varicella vaccine. In a large-scale clinical trial among approximately 40,000 adult, elderly subjects age 60 years or older, Oxman *et al.* reported that Zostavax (a Varicella vaccine) reduced onset of shingles to roughly one-half, and PHN to approximately one-third[28]. Inoculation of 22,439 adult subjects age 50-59 years with Zostavax was also found to reduce shingles by approximately 70% in a 1-year or longer observational period. Based on these results, Zostavax was found to be indicated in the

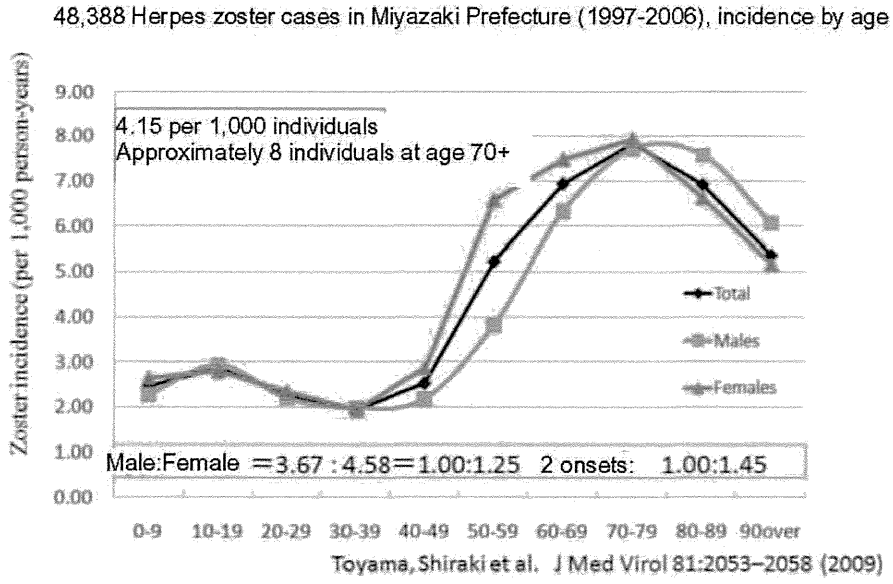

Fig. 5. **48,388 Herpes zoster cases in Miyazaki Prefecture (1997-2006), incidence by age**

US for prevention of shingles among individuals age 50 or older.

While inoculation with measles/rubella vaccines can prevent measles and rubella almost entirely, Zostavax prevents shingles roughly to a half, but onset still occurs half despite vaccination. Considering the fact that the effect of anti-herpes drugs used to treat shingles is to possibly shorten the treatment interval by 1 day, the reduction of incidence to a half is a significantly more benefical effect than antiviral therapy. However, patients should be advised that measles and rubella may occur even with vaccination in a milder form than without vaccination.

Though the Varicella vaccine used in Japan is deemed to have an immunostimulatory activity for VZV, this vaccine is presently not licensed for prevention of shingles.

Finally, both the Japanese Varicella vaccine and Zostavax for prevention of shingles were manufactured within 10 generations from the original Oka strain of the Varicella vaccine developed in Japan, and the vaccine strains are regarded as the same in immunogenicity or other such properties. The Varicella vaccine used in Japan also has a titer equivalent to that of Zostavax. Consequently, commercial Varicella vaccines are presently not licensed but are deemed to provide a shingles-preventive effect equivalent to that of Zostavax.

4) Immunosuppressant research from the Zizimin2 gene perspective

Techniques for comparison of young and elderly strata have attracted recent attention to research on mechanisms of fragile immunity as an age-related change in biological functions at the cellular level, primarily in lymphocytes, and at the individual level in mice and humans. Just as in the nervous and endocrine systems, immunocompetence is also known to decline with aging and senescence, and changes in acquired immunity, primarily among lymphocytes, are regarded as intimately related to rates of contraction and the progress and prognosis for many diseases that involve the elderly.

Under a mission of "Understanding immunosenescence mechanisms", we are therefore pursuing research to investigate changes in cell populations and gene expression specific to various immune systems in the body; understand fluctuations in cytokines and other endocrine proteins and the associated mechanisms; maintain immunocompetence in the elderly; standardize levels of immunosenescence to infectious disease, even preventively; and improve age-related changes in gut immunity and body defense functions through perspectives including nutritional intervention.

In this paper, we introduce one aspect of immunosenescence research at this molecular level. We also report on Zizimin2/Dock11 molecular level function of the novel guanine nucleotide exchange factor (GEF), and we report a functional analysis and other information relating to acquired immune system senescence and infectious disease at the individual level, in research using Zizimin2 gene knockout mice.

Zizimin2 (Ziz2) is of interest as an immunosenescence-related gene isolated and identified from B cells in the germinal center of the mouse spleen. It belongs to the Zizimin family, a CDM (CED-5, DOCK180, Myoblast city) family [29-31], and was shown to function as a guanine nucleotide exchange factor which binds to and activates Rho family GTPase and cdc42 through a CZH2 domain [32]. Rats were then immunized with a Ziz2 C-terminal recombinant protein as an antigen, the hybridoma strain obtained was selected by ELISA, and antibodies specific to the CZH2 domain of Ziz2 (214) were obtained, along with antibodies reactive to the CZH2 domain of Ziz2 and Zizl (126).

Using these antibodies, we introduce results for a functional analysis of the Ziz2 molecule in dendrite cells, an important immunocompetent cell for such processes as conventional intracellular localization, antigen presentation, chemokine-dependent migration, and antigen phagocytosis.

First, Ziz2 protein expression was found to be specific to immune system tissues (*e.g.*, spleen, thymus), as in the case of gene expression. *In vitro* functional analysis of immunocompetent cells using aged C57BL6 mouse individuals (age 24 months) was then performed to compare changes in lymphocyte count as an age-related change in immune system tissues, and expression of Ziz2 proteins was found to have declined dramatically. Forced expression of the entire Ziz2 length in 293T cells demonstrated formation of filopodia and showed that Ziz2 was present within the cells and on cell membranes. The fact that migration to the vicinity of the cell membrane, including migration of these projections, was not observed in forced expression of the CZH2 domain alone, was a result suggesting that migration to the cell membrane involves binding with Cdc42 and function of non-CZH2 domain portions having activated domains [33] .(***Fig. 6***)

To express Ziz2 by anti-FcγRII/III and LPS stimulation in dendrite cells, we first cultured bone marrow cells for 8 days in the presence of mGM-CSF to induce bone marrow-derived cells (BMDC). On Day 8, Western blotting was used to compare expression of Ziz2 after stimulation of cells with anti-FcγRII/III (2.4G2) and anti-rat IgG Fab'2, LPS, or anti-CD40. The results showed that transient expression of Ziz2 increased when BMDC were activated by anti-FcγRII/III antibodies or LPA and at the same time ascertained transient activation of intrinsic GTP-type cdc42. These results in BMDC correspond closely to the fact that Ziz2 is present downstream from TLR4 or FcγR signaling.

Ziz2 gene knockout mice were also produced to elaborate age-related and other changes in response to infection from the standpoint of their role in natural immune systems and its bearing on clinical research. In the future, we hope to use these mice for *in vivo* analysis intended to create an initial understanding of age-related weakening of immune response.

Conclusion

What began with calls in the 1970s for recognition of an aging society became a truly aging society in 2008, when 1 in 5 individuals was elderly, and 1 in 10 individuals was highly elderly. Fifty years from now, by some calculations, 1 in 2.5 individuals will be elderly. Anti-Aging Medicine is by no means intended to inhibit aging itself. As the perspective of the Study Committee for Revision of Senior Health Maintenance Initiatives (October 2004) indicated in its phrase "From a 'Healthy 65' to an 'Active 85'", the need is to envision "a new image of the elderly allowing active, meaningful self-fulfillment even while living with illness", and whenever possible, it is crucial to raise the number of "mobile 85-year-olds" engaged in healthy longevity. This translates, in other words, to improved QOL among the elderly and treatment (including prevention) for age-related diseases.

Here we introduce a variety of approaches. Therapies specifically controlling just some pathologies through understanding of molecular mechanisms, control of immune response, immunosuppression, immune strengthening, and other such approaches represent safe and effective, appealing

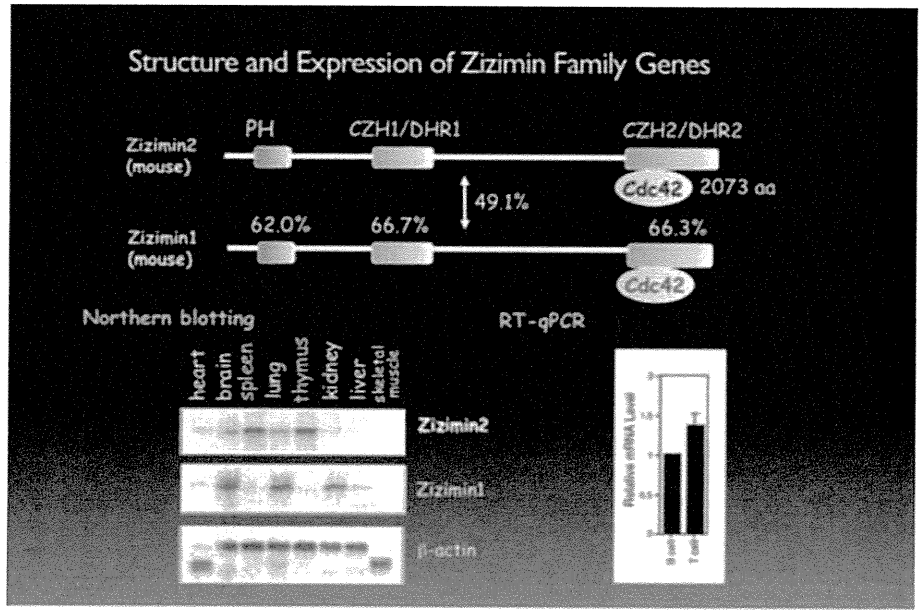

Fig. 6. **Specificity of Zizimin family gene structure and expression**
Zizimin1 and 2 show overall high homology centered on the functional domain, but their gene expression formats are complementary, and Zizimin2 demonstrates specificity of expression in a broad range of immune tissues.

therapeutic modalities. Though immune mechanisms are acquired by higher animals to distinguish between self and non-self and protect the body from infection, recognition of self versus non-self can then become a trigger for autoimmune disease. In general, the body defense functions of elderly individuals present many problems with regard to monitoring of non-self and tolerance of self, and maintenance of that balance, *i.e.*, homeostasis is all-important. With great expectations, we look forward to future developments in research and results from clinical application.

Conflicts of Interest:

The authors declare no financial or other conflicts of interest in the writing of this paper.

References

1) Miyazawa M ,et al :Human Pathology- mechanism of disease- ; Aozasa K.,ed. Ishiyaku Publishers Inc., 83-129:2009
2) Miyazawa M, Tsuji-Kawahara S, Kanari Y: Host genetic factors that control immune responses to retrovirus infections. Vaccine 26; 2981-2996: 2008
3) Chesebro B, Miyazawa M, Britt WJ: Host genetic control of spontaneous and induced immunity to Friend murine retrovirus infection. Annu Rev Immunol 8; 477-499: 1990
4) Takeda E, Tsuji-Kawahara S, Sakamoto M, et al: Mouse APOBEC3 restricts Friend leukemia virus infection and pathogenesis *in vivo*. J Virol 82; 10998-11008: 2008
5) Tsuji-Kawahara S, Chikaishi T, Takeda E, et al: Persistence of viremia and production of neutralizing antibodies differentially regulated by polymorphic APOBEC3 and BAFF-R loci in Friend virus-infected mice. J Virol 84; 6082-6095: 2010
6) Ogawa T, Tsuji-Kawahara S, Yuasa T, et al: Natural killer cells recognize Friend retrovirus-infected erythroid progenitor cells through NKG2D-RAE-1 interactions *in vivo*. J Virol 85; 5423-5435: 2011
7) Iwashiro M, Kondo T, Shimizu T, et al: Multiplicity of virus-encoded helper T-cell epitopes expressed on FBL-3 tumor cells. J Virol 67; 4533-4542: 1993
8) Kondo T, Uenishi H, Shimizu T, et al: A single retroviral gag precursor signal peptide recognized by FBL-3 tumor-specific cytotoxic T lymphocytes. J Virol 69; 6735-6741: 1995
9) Sugahara D, Tsuji-Kawahara S, Miyazawa M: Identification of a protective CD4+ T-cell epitope in p15gag of Friend murine leukemia virus and role of the MA protein targeting to the plasma membrane in immunogenicity. J Virol 78; 6322-6334: 2004
10) Miyazawa M, Fujisawa R, Ishihara C, et al: Immunization with a single T helper cell epitope abrogates Friend virus-induced early erythroid proliferation and prevents late leukemia development. J Immunol 155; 748-758: 1995
11) Iwanami N, Niwa A, Yasutomi Y, Tabata N, Miyazawa M. Role of natural killer cells in resistance against Friend retrovirus-induced leukemia. J Virol 75; 3152-3163: 2001
12) Kawabata H, Niwa A, Tsuji-Kawahara S, et al, Miyazawa M: Peptide-induced immune protection of CD8+ T cell-deficient mice against Friend retrovirus-induced disease. Int Immunol 18; 183-198: 2006
13) Takamura S, Tsuji-Kawahara S, Yagita H, et al: Premature terminal exhaustion of Friend virus-specific effector CD8+ T cells by rapid induction of multiple inhibitory receptors. J Immunol 184; 4696-4707: 2010
14) Takamura S, Miyazawa M: Response to comment on "Premature terminal exhaustion of Friend virus-specific effector CD8+ T cells by rapid induction of multiple inhibitory receptors." J Immunol 185; 1349-1350: 2010
15) Noon L: Prophylactic inoculation against hay fever. Lancet 1; 1572-1573: 1911
16) Mirone C, Albert F, Tosi A, et al: Efficacy and safety of subcutaneous immunotherapy with a biologically standardized extract of Ambrosia artemisiifdia pollen in double-blind placebo controlled study. Clin Exp Allergy 34; 1408-1414: 2004
17) Durham SR, Emminger W, Kapp A, et al: Long-term clinical efficacy of grass-pollen immunotherapy. N Engl J Med 341; 468-475: 1999
18) Maestrelli P, Zanolla L, Pozzan M, Fabbri LM: Regione Veneto Study Group on the "Effect of immunotherapy in allergic asthma": Effect of specific immunotherapy added to pharmacologic treatment and allergen avoidance in asthmatic patients allergic to house dust mite. J Allergy Clin Immunol 111; 643-649: 2004
19) Ameal A, Vega-Chicote JM, Fernández S, et al: Double-blind and placebo-controlled study to assess efficacy snd safety of modified allergen extract of Dermatophagoides Pteronissinus in Allergic asthma. Allergy 60; 1178-1183: 2005
20) Pifferi M, Baldini G, Marrazzini G, et al: Benefits of immunotherapy with a standardized Dermatophagoides pteronyssinus extract in asthmatic children: a three years prospective study. Allergy 57; 785-790: 2002
21) Möller C, Dreborg S, Ferdousi HA, et al: Pollen immunotherapy reduces the development of asthma in children with seasonal rhinoconjunctivitis (the PAT-study). J Allegy Clin Immunol 109; 251-256: 2002
22) Gotoh M, Okubo K: Sublingual immunotherapy for Japanese cedar pollinosis. Allergology International 54; 167-171: 2005
23) Okubo K, Gotoh M, Fujieda S, Okano M et al: A randomized double-blind comparative study of sublingual immunotherapy for cedar pollinosis. Allergol Int 57; 265-275: 2008
24) Toyama N, Shiraki K: Epidemiology of herpes zoster and its relationship to varicella in Japan: A 10-year survey of 48,388 herpes zoster cases in Miyazaki prefecture. J Med Virol 81;2053-2058: 2009
25) Opstelten W, Mauritz JW, de Wit NJ, van Wijck AJ, Stalman WA, van Essen GA: Herpes zoster and postherpetic neuralgia: incidence and risk indicators using a general practice research database. Fam Pract 19; 471-475: 2002
26) Hope-Simpson RE: The Nature of Herpes Zoster: A Long-Term Study and a New Hypothesis. Proc R Soc Med 58; 9-20: 1965
27) Yih WK, Brooks DR, Lett SM, et al: The incidence of varicella and herpes zoster in Massachusetts as measured by the Behavioral Risk Factor Surveillance System (BRFSS) during a period of increasing varicella vaccine coverage, 1998-2003. BMC Public Health 5; 68: 2005
28) Oxman MN, Levin MJ, Johnson GR, et al: A vaccine to prevent herpes zoster and postherpetic neuralgia in older adults. N Engl J Med 352; 2271-2284: 2005
29) Tosello-Trampont AC, Macara IG, Madhani H, Fink GR and Ravichandran KS: Unconventional Rac-GEF activity is mediated through the Dock180 ELMO complex. Nat Cell Biol 4; 574-582: 2002
30) Cote JF, Vuori K: Identification of an evolutionarily conserved superfamily of DOCK180-related proteins with guanine nucleotide exchange activity. J Cell Sci 115; 4901-4913: 2002
31) Meller N, Irani-Tehrani M, Kiosses WB, Del Pozo MA, Schwartz MA: Zizimin1, a novel Cdc42 activator, reveals a new GEF domain for Rho proteins. Nat Cell Biol 4; 639-647: 2002
32) Nishikimi A, Meller N, Uekawa N, Isobe K, Schwartz MA, Maruyama M: Zizimin1, a novel Cdc42 activator, reveals a new GEF domain for Rho proteins. FEBS Lett 579; 1039-1046: 2005
33) Meller N, Merlot S, Guda C: CZH proteins: a new family of Rho-GEFs. J Cell Sci 118; 4937-4946: 2005

Glycoconj J (2012) 29:77–85
DOI 10.1007/s10719-011-9366-x

Critical roles of Asp270 and Trp273 in the α-repeat of the carbohydrate-binding module of endo-1,3-β-glucanase for laminarin-binding avidity

Tomonari Tamashiro · Yoichi Tanabe · Teikichi Ikura · Nobutoshi Ito · Masayuki Oda

Received: 14 September 2011 / Revised: 9 December 2011 / Accepted: 15 December 2011 / Published online: 27 December 2011

Abstract A carbohydrate-binding module from family 13 (CBM13), appended to the catalytic domain of endo-1,3-β-glucanase from *Cellulosimicrobium cellulans*, was overexpressed in *E. coli*, and its interactions with β-glucans, laminarin and laminarioligosaccharides, were analyzed using surface plasmon resonance biosensor and isothermal titration calorimetry. The association constants for laminarin and laminarioligosaccharides were determined to be approximately 10^6 M^{-1} and 10^4 M^{-1}, respectively, indicating that 2 or 3 binding sites in the α-, β-, and γ-repeats of CBM13 are involved in laminarin binding in a cooperative manner. The binding avidity is approximately 2-orders higher than the monovalent binding affinity. Mutational analysis of the conserved Asp residues in the respective repeats showed that the α-repeat primarily contributes to β-glucan binding. A Trp residue is predicted to be exposed to the solvent only in the α-repeat and would contribute to β-glucan binding. The α-repeat bound β-glucan with an affinity of approximately 10^4 M^{-1}, and the other repeats additionally bound laminarin, resulting in the increased binding avidity. This binding is unique compared to the recognition mode of another CBM13 from *Streptomyces lividans* xylanase.

T. Tamashiro · Y. Tanabe · M. Oda (✉)
Graduate School of Life and Environmental Sciences, Kyoto Prefectural University,
1-5 Hangi-cho, Shimogamo, Sakyo-ku,
Kyoto 606-8522, Japan
e-mail: oda@kpu.ac.jp

T. Ikura · N. Ito
Graduate School of Biomedical Science, Tokyo Medical and Dental University,
1-5-45 Yushima, Bunkyo-ku,
Tokyo 113-8510, Japan

Keywords Carbohydrate-binding module · β-glucan · Affinity and avidity · Site-directed mutagenesis · Biomolecular interaction

Abbreviations

CBM	Carbohydrate-binding module
SPR	Surface plasmon resonance
ITC	Isothermal titration calorimetry
His-tag	Polyhistidine-tag
PCR	Polymerase chain reaction
Ni-NTA	Ni-nitrilotriacetic acid
SDS-PAGE	Sodium dodecyl sulfate-polyacrylamide gel electrophoresis
CD	Circular dichroism
DLS	Dynamic light scattering

Introduction

The carbohydrate-binding module (CBM) is defined as a contiguous amino-acid sequence within a carbohydrate-active enzyme with a discrete fold having carbohydrate-binding activity [1–3]. To date, CBMs have been classified into 64 different families based on amino-acid sequence, binding specificity, and ternary structure [3]. They are considered to have a critical function in localizing the connected enzymes to their substrates [4]. In addition to their biological function, CBMs are good targets for the analysis of carbohydrate recognition mechanisms. We recently cloned a gene encoding the endo-1,3-β-glucanase from the genomic DNA of *Cellulosimicrobium cellulans* DK-1 and found that the enzyme has a catalytic domain and a CBM family 13 (CBM13), named CBM-DK, connected by a Gly/Ser-rich linker region [5]. Compared with the structures of other

CBM13s from *Streptomyces lividans* xylanase 10A and *Streptomyces olivaceoviridis* E-86 xylanase, whose crystal structures are available [6–8], 6 Cys residues are conserved and are predicted to form disulfide bonds (Fig. 1). CBM13s have a β-trefoil fold displaying the pseudo-3-fold symmetry arising from imperfect tandem α-, β-, and γ-repeats. Previous studies of CBM13 from *Streptomyces lividans* xylanase 10A have shown that each repeat has a xylan binding site, and that the 3 binding sites interact with xylan in an additive and cooperative manner [10]. It has also been shown that the conserved Asp residues, Asp19, Asp61, and Asp102 (Fig. 1), located in the α-, β-, and γ-repeats, respectively, participate in xylan binding through hydrogen bonding [6, 11]. In CBM-DK, Asp270, Asp311, and Asp355 correspond to the conserved Asp residues (Fig. 1), and are predicted to participate in β-glucan binding. In addition, it seems that a unique hydrophobic residue, Trp273, located in the α-repeat, would be exposed to the solvent and interact with β-glucan,

(a)

```
                 260              270              280              290              300
CBM-DK     GTGA VRAA=NGMCVD VPWADPTDGN PVQIVTCSGN AAQTWTRGSD
                  8               19               29               39               49
CBM-SlXy   DG-Q IKGVGS-R-L- --D-STS--T QL-LWD-HSG TN-Q-AATDA
                314              325              335              345              355
CBM-SoXy   -G-Q IKGVGS-R-L- --N-ST---T Q--LYD-HSA TN-Q--YTDA

                        310              320              330              340
CBM-DK      GTVRALG=KCL DVRDGSTTRG AAVQVWTCNG TGAQLWAYDA GS
                         60               68               78               88
CBM-Xy     -EL-VY-D--- -A==AG-SN- SK--IYS-W- GDN-K-RLNS DG
                        366              374              384              394
CBM-SoXy   -EL-VY-D--- -A==AG-GN- TK--IYS-W- GDN-K-RLNS DG

                   350              360              370              380
CBM-DK     KALRNPQS GLCLDATGGA PLHDGQRLQT WTCNGTTAQQ WTL
                    97              107              116              126
CBM-Xy     SVV=GV-- --------V-NG TA=N-TLI-L Y--SNGSN-R --RT
                   403              413              422              433
CBM-SoXy   SIV=GV-- --------V--G TA=N-TLI-L YS-SNGSN-R --RT
```

(b)

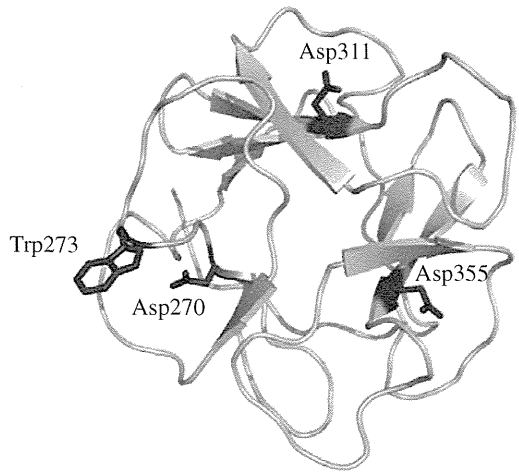

Fig. 1 Structural comparison and model of CBM-DK. **a** Comparison of the amino acid sequences of CBM-DK with CBM13s from *Streptomyces lividans* xylanase 10A (CBM-SlXy) and *Streptomyces olivaceoviridis* E-86 xylanase 10A (CBM-SoXy). Single dashes denote identity to CBM-DK, and double dashes indicate no amino acid residue at that position. The conserved Cys residues are boxed, and the substituted residues, Asp270, Trp273, Asp311, and Asp355, are in italic. The homologies of CBM-DK with CBM-SlXy and CBM-SoXy are 35% and 37%, respectively. **b** The 3D structural model of CBM-DK. The model was created with Swiss-Model [9], using the X-ray crystal structure of CBM-SoXy (PDB ID; 1V6W) [8]. The four mutated residues, Asp270, Trp273, Asp311, and Asp355, are explicitly shown

based on the previously reported crystal structures of CBM13s [6–8]. The corresponding residues in the β- and γ-repeats are Asp314 and Gly358, respectively (Fig. 1).

In this study, we overexpressed CBM-DK, corresponding to Gly257-Leu383 of endo-1,3-β-glucanase from *Cellulosimicrobium cellulans* DK-1, in *E. coli* with an N-terminal polyhistidine-tag (His-tag). In order to determine the quantitative effect of additive and cooperative interaction with β-(1-3)-glucans, the binding of CBM-DK to both laminarin and laminarioligosaccharides was analyzed using surface plasmon resonance (SPR) biosensor and isothermal titration calorimetry (ITC). Because the laminarin from *Laminaria digitata* used in this study has an average molecular weight of 6 k and the ratio of β-(1-3) to β-(1-6) linkages is 7:1 [12], it can interact with CBM-DK in a multivalent manner. Although the multivalent binding is considered to increase the binding strength due to the avidity effect [13], the quantitative correlation between affinity and avidity is poorly understood, particularly for carbohydrate binding. The second purpose of this study was to elucidate the role of each repeat in CBM-DK in β-glucan binding. In order to determine whether or not the contribution of each repeat is equal, the conserved Asp residues, Asp270, Asp311, and Asp355, located in the α-, β-, and γ-repeats were mutated to Ala, individually or in combination, and the binding affinities of the mutants for laminarin and laminarioligosaccharides were compared. Together with the results with the W273S mutant, we found that the α-repeat primarily contributes to β-glucan binding, which is different from the case of CBM13 of xylanase.

Materials and methods

Materials

Laminarin from *Laminaria digitata* and laminarioligosaccharides from *Poria cocos* were purchased from Sigma-Aldrich Co. (USA) and Seikagaku Kogyo Co. (Japan), respectively. The plasmid vector, pET28-a (Novagen, USA), was used for expression of proteins.

Expression and purification of CBM-DK

The DNA region encoding CBM-DK was first amplified as *NdeI*/*Eco*RI fragments by polymerase chain reaction (PCR) using the primer pairs F1 and R1 (F1; 5′-GTCGGCCCATA TGGGGACCGGCGCGGTG-3′, R1; 5′-GCGAATT CTCAGAGCGTCCACTGCTGGGC-3′) and the genomic DNA from *Cellulosimicrobium cellulans* DK-1 as the template [5]. The resultant PCR products were then cloned into the pET28-a expression vector that encodes an N-terminal His-tag. Site-directed mutagenesis was performed by overlap extension PCR methods [14]. In this study, CBM-DK wild-type with an N-terminal His-tag is simply referred to as CBM-DK, and its mutant is referred to as the substituted residue name (*e.g.*, D270A stands for the mutant in which Asp270 was substituted with Ala).

Recombinant *E. coli* BL21(DE3) harboring the expression vector containing either CBM-DK or its mutants were grown at 37°C in Luria-Bertani medium to mid-log phase, and isopropyl-β-thiogalactoside was added to a final concentration of 0.1 mM to induce protein expression. After an additional incubation of 4 h at 37°C, the bacteria were harvested, resuspended in 20 mM potassium phosphate buffer (pH 8.0) containing 300 mM NaCl, and sonicated. Because the overexpressed CBM-DK protein was insoluble, it was solubilized in 20 mM potassium phosphate buffer (pH 8.0) containing 8 M urea, and refolded by stepwise dialysis in 0.2 mM oxidized glutathione, 2 mM reduced glutathione, and 20 mM potassium phosphate buffer (pH 8.0) containing 2 M, 1 M, and 0 M urea, in succession, at 4°C. The refolded protein was loaded onto a Ni-nitrilotriacetic acid (Ni-NTA) column and eluted using 20 mM potassium phosphate buffer (pH 8.0) containing 300 mM NaCl and 500 mM imidazole. The sodium dodecyl sulfate-polyacrylamide gel electrophoresis (SDS-PAGE) analysis was carried out using a 15% separating gel, and the resultant protein bands were stained with Coomassie brilliant blue. The purified protein concentrations were calculated from absorbance values recorded at 280 nm, using the extinction coefficient of 2.05 ml mg^{-1} cm^{-1}.

Circular dichroism (CD) spectrometry

The purified proteins were dialyzed against 40 mM potassium phosphate buffer (pH 7.0) at 4°C. The far-UV CD spectra were measured on JASCO J-720 spectrometer, using a scan speed of 20 nm/min, a time response of 1 s, a bandwidth of 1 nm, an average over 8 scans, and a cell with 0.2 cm optical path length.

Dynamic light scattering (DLS) measurement

Zetasizer μV (Malvern Instruments Ltd.) was used for measuring DLS to analyze the oligomeric state of CBM-DK in 40 mM potassium phosphate buffer (pH 7.0) at 25°C. The measurement was performed using a laser beam of 830 nm at an angle of 90°.

SPR measurement

The Biacore biosensor system, Biacore 2000 (GE Healthcare Bioscience, Uppsala, Sweden), was used to measure real-time β-glucan interactions. CBM-DK and its mutants were covalently linked to sensor chip, CM5, and β-glucans

with various concentrations in 10 mM phosphate buffer (pH 7.3) containing 0.14 M NaCl and 0.005% Tween20 were applied over the sensor chip at a rate of 20 μl/min during 3 min. The surface was regenerated with one 15 μl injection of a solution of 10 mM acetic acid buffer (pH 4.0). All experiments were performed at 25°C.

The sensorgrams for β-glucan and CBM-DK interactions were examined by first adjusting for background changes reflected by the bulk refractive indices, and were next analyzed using BIA evaluation 3.2 software. The equilibrium association constant (K_a) values were determined by Scatchard analysis using Eq. 1:

$$RU_{eq}/C = K_a \times RU_{max} - K_a \times RU_{eq} \quad (1)$$

where C is the free analyte concentration, RU_{eq} is the steady-state response, and RU_{max} is the total surface binding capacity.

ITC measurement

ITC experiments were carried out on an iTC200 calorimeter interfaced with a microcomputer (GE Healthcare Bioscience, Uppsala, Sweden). All samples were in 40 mM phosphate buffer (pH 7.0), and all solutions were thoroughly degassed. The solution of laminarin or laminarioligosaccharides was titrated into the CBM-DK solution using a 40-μl syringe. Each titration consisted of a preliminary 0.3-μl injection followed by 29 subsequent 1.3-μl additions. The heat for each injection was subtracted from the dilution heat of the titrant, measured by injecting the β-glucan solution into buffer alone. Each corrected heat was divided by the moles of β-glucan injected. Data were analyzed using the Origin software supplied by GE Healthcare Bioscience.

Results

The cDNA encoding CBM-DK was successfully amplified by PCR, using genomic DNA from *Cellulosimicrobium cellulans* as the template, and cloned into the pET28-a vector. The plasmids encoding CBM-DK mutants were constructed by site-directed mutagenesis. CBM-DK and its mutants with an N-terminal His-tag were overexpressed in *E. coli*, and most of the protein was in the insoluble fraction (Fig. 2a). The protein was solubilized by the addition of urea and refolded by the step-wise dilution of urea. The solubilized and refolded protein was purified using a Ni-NTA affinity column (Fig. 2a). The far-UV CD spectrum of purified CBM-DK indicated that it had folded correctly (Fig. 2b) and agreed with the postulated β-strand-rich structure, as observed in the crystal structures of CBM13s at the C-terminal modules of xylanases [6–8]. In the DLS analysis, one size distribution

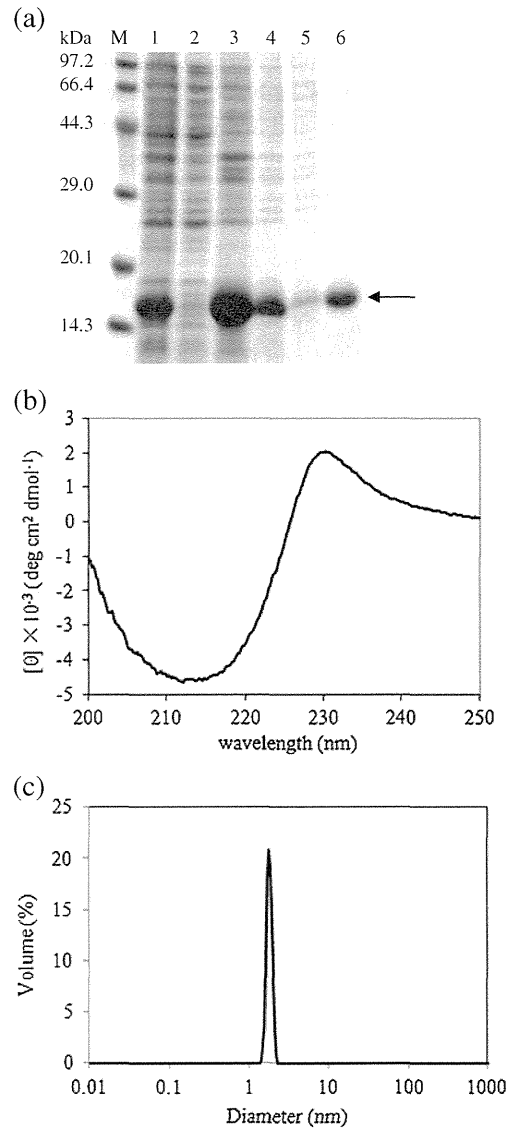

Fig. 2 Purification and structural analysis of CBM-DK. **a** SDS-PAGE analysis after each purification step. Lanes: M, standard molecular weight marker; 1, crude extract; 2, soluble fraction after sonication; 3, solubilized fraction using 8 M urea; 4, refolded fraction after dialysis; 5, flow through fraction from Ni-NTA affinity column; 6, the eluted protein from Ni-NTA affinity column. The arrow indicates the band of CBM-DK (15. 4 kDa). **b** Far-UV CD spectrum of 13 μM CBM-DK. **c** Size distribution by mass of 20 μM CBM-DK analyzed using DLS

by mass was observed for CBM-DK, in which the molecular mass was estimated to be 13.9±1.1 kDa (Fig. 2c), indicating that CBM-DK exists as a monomer. This is also supported by the results of gel-filtration HPLC analysis (data not shown).

Binding of laminarin was analyzed by SPR using a sensor chip on which CBM-DK was immobilized. When a protein is immobilized by amine coupling, the amino group exposed to the solvent becomes immobilized. To eliminate the possibility that the binding surface of CBM-DK was masked and interfering with β-glucan binding when

immobilized, another CBM-DK with an additional Lys at the N-terminus was immobilized on the sensor chip, and its binding to β-glucans was analyzed. The results showed that the binding sensorgrams and affinity to laminarin and laminarioligosaccharides were similar to those of immobilized CBM-DK. Figure 3a shows typical sensorgrams for the binding of laminarin to CBM-DK. In Scatchard plots (Fig. 3b), a gradual increase in the slope at a lower occupancy was observed, indicating the existence of different binding modes. The K_a values determined from the linear fit in the range of 5–40 μM and 0.625–5 μM of laminarin are 1.1×10^6 M^{-1} and 8.0×10^6 M^{-1}, respectively (Table 1). Because CBM-DK has 3 binding sites and was immobilized on the sensor chip, the multivalent binding to laminarin should have occurred on not only a CBM-DK molecule but simultaneously on multiple CBM-DK molecules in addition to the monovalent binding that took place. In order to distinguish the avidity effect derived from immobilization of multiple CBM-DK molecules, ITC measurements were carried out. Figure 4 shows a typical ITC profile for the

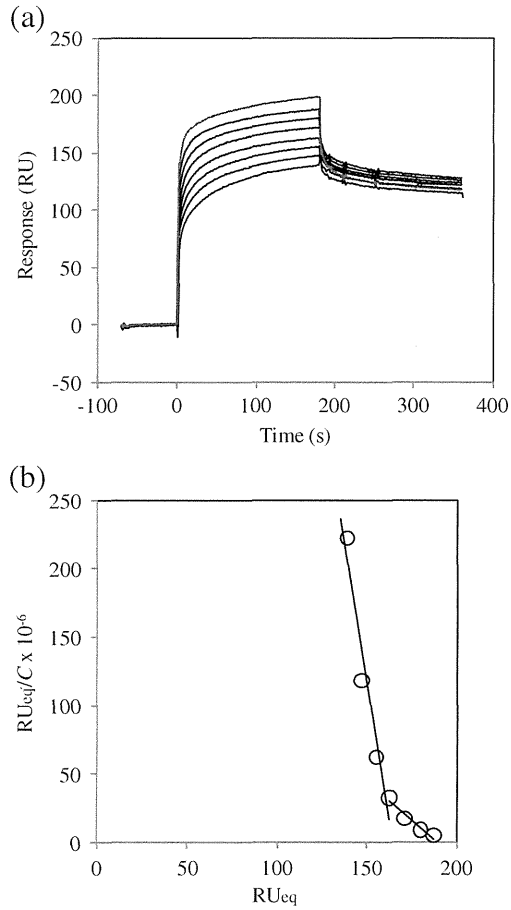

Fig. 3 SPR analysis of interactions between laminarin and immobilized CBM-DK. **a** Sensorgrams for the binding of laminarin (0.625–40 μM). **b** Scatchard plots for the binding of laminarin. The K_a values determined from the linear fitting to the laminarin in the range of 5–40 μM and 0.625–5 μM, respectively

binding of laminarin to CBM-DK. The thermodynamic parameters obtained are summarized in Table 2. From the assumption that each CBM-DK binds to laminarin independently, the K_a value 1.32×10^6 M^{-1} corresponds to the binding strength derived from a single CBM-DK molecule. A binding stoichiometry (n) of 0.12 indicates that approximately 8 CBM molecules bind to a single laminarin molecule. The binding reactions are enthalpy-driven.

The binding of laminarioligosaccharides was analyzed by both SPR and ITC. Scatchard plots for the laminarioligosaccharides generated straight lines, in which K_a values for the binding of laminaritetraose and laminarihexaose obtained from the slopes were 1.5×10^4 M^{-1} and 2.8×10^4 M^{-1}, respectively (Table 1), which were comparable to those obtained by ITC (Table 2). The observed binding is expected to be monovalent, and the K_a values are about 2-orders lower than that for laminarin binding. The n value of ~1 indicates that the laminarioligosaccharide binds to one of the 3 sites on CBM-DK, with the observed heat.

In order to determine the role of each repeat of CBM-DK in β-glucan binding, 3 Asp residues, Asp270, Asp311, and Asp355, were mutated to Ala, individually or in combination, and the β-glucan binding of each mutant was analyzed by SPR. The K_a values obtained are summarized in Table 1. In both binding to laminarioligosaccharides and binding to laminarin, no increase in RU was observed for the mutants D270A, D270A/D311A, or D270A/D355A, while the K_a values for the mutants D311A, D355A, and D311A/D355A were similar to those for CBM-DK. The results clearly indicate that the α-repeat is more critical than the other 2 repeats for β-glucan binding. In addition, the decreased K_a value for laminarin binding of W273S supports the proposed role of the α-repeat. While little increase in RU was observed for D270A with the laminarin concentrations analyzed, an increase in RU was observed for W273S, indicating that the contribution of Asp270 to β-glucan binding is larger than that of Trp273. In order to analyze the laminarin binding in a single D311A/D355A molecule, the ITC measurement was carried out. The K_a value determined was lower than that of CBM-DK wild-type (Table 2), which would be due to the decreased contribution of β- and/or γ-repeats.

Discussion

Several binding mechanisms should be considered for the interactions of CBM-DK with laminarin and laminarioligosaccharides (Fig. 5). In the interaction between laminarin and CBM-DK immobilized on the flexible dextran surface of SPR sensor chip, multiple CBM-DK molecules could be involved. One of the advantages of using this system is that the molecular interaction with a low binding affinity could be observed, due to the avidity effects. In the low

Table 1 K_a values (M^{-1}) for interactions of β-glucans with immobilized CBM-DK and its mutants on the sensor chip

CBM	Laminaritetraose[a]	Laminarihexaose[b]	Laminarin[c]	Laminarin[d]
CBM-DK	1.5×10^4	2.8×10^4	8.0×10^6	1.1×10^6
D270A	n.d.[e]	n.d.[e]	n.d.[e]	n.d.[e]
W273S	n.d.[e]	n.d.[e]	7.9×10^5	1.8×10^5
D311A	3.3×10^3	2.1×10^4	1.3×10^7	1.6×10^6
D355A	2.6×10^3	1.7×10^4	7.4×10^6	1.4×10^6
D270A/D311A	n.d.[e]	n.d.[e]	n.d.[e]	n.d.[e]
D270A/D355A	n.d.[e]	n.d.[e]	n.d.[e]	n.d.[e]
D311A/D355A	5.2×10^3	3.8×10^4	2.4×10^7	–
D270A/D311A/D355A	n.d.[e]	n.d.[e]	n.d.[e]	n.d.[e]

[a] Determined from a Scatchard analysis using laminaritetraose concentrations of 0.16–1.28 mM

[b] Determined from a Scatchard analysis using laminarihexaose concentrations of 0.08–0.64 mM

[c] Determined from a Scatchard analysis using laminarin concentrations of 0.625–5 μM

[d] Determined from a Scatchard analysis using laminarin concentrations of 5–40 μM

[e] Not determined from the sensorgram because little increase of RU was observed

concentration of laminarin, 3 or more binding sites in multiple CBM-DK molecules could be involved in laminarin binding (Fig. 5e), resulting in a higher binding strength than that observed by ITC. In the high concentration of laminarin, 2 or 3 binding sites in CBM-DK molecule(s) are predicted to be involved (Fig. 5d). In contrast, the K_a value obtained by ITC is expected to be derived from the interaction of a single CBM-DK molecule because ITC detects the heats of interactions in solution. The K_a value for laminarin binding was determined to be 1.32×10^6 M^{-1}, which is comparable to the K_a value determined using laminarin at concentrations of 5–40 μM in the SPR experiments, and is about 2-orders higher than the binding affinity for laminarioligosaccharides (Tables 1 and 2). Taken together, the results indicate that CBM-DK interacts with laminarioligosaccharides in a monovalent manner, while it interacts with laminarin in a multivalent manner. Possibly due to the flexibility and/or the branch of the β-(1-6) linkage, a laminarin molecule could simultaneously bind to 2 or 3 binding sites within a single CBM-DK molecule (Fig. 5b).

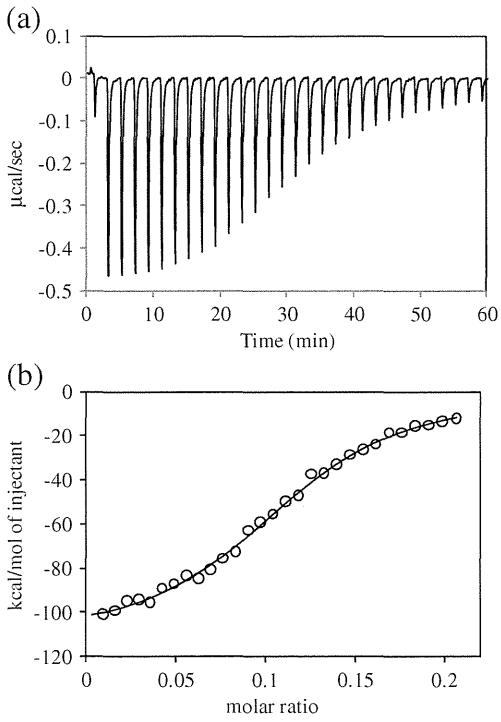

Fig. 4 ITC analysis of interactions between laminarin and CBM-DK. **a** The 60 μM laminarin solution was injected 30 times in 1.3-μl increments into the 60 μM CBM-DK solution. Data were obtained at 25°C. **b** The data points were obtained by integration of the peaks in (**a**), corrected for the dilution heat, and plotted against the molar ratio, laminarin/CBM-DK. The data were fitted using a nonlinear least-squares method

The present mutational analysis clearly showed that the contribution of each binding site of the α-, β-, and γ-repeats to β-glucan binding is nonequivalent, which is not the case with CBM13 of *Streptomyces lividans* xylanase 10A [10]. No increase in RU was observed for the binding of Asp270 mutants to laminarin and laminarioligosaccharides (Table 1), indicating that the α-repeat primarily contributes to β-glucan binding. In the mutant of D311A/D355A, because laminarin is long enough to interact with multiple CBM molecules as described below, 3 or more α-repeats of adjacent D311A/D355A molecules immobilized on the SPR sensor chip would be involved in laminarin binding, resulting in the K_a value similar to that of CBM-DK wild-type (Table 1). The decreased binding affinity of the W273S mutant also supports the critical role of the α-repeat. In the amino-acid sequence, there is a unique hydrophobic residue, Trp273, within the α-repeat. The corresponding residue in the CBM13 α-repeat of *Streptomyces lividans* xylanase 10A is Asp22 (Fig. 1a), and it contributes to carbohydrate binding [6]. Taken together, Trp273 could participate in binding to

Table 2 Thermodynamic parameters of β-glucan binding to CBM-DK and D311A/D355A

β-glucan	*n*	K_a (M^{-1})	$\Delta G°$	ΔH (kcal·mol^{-1})	$T\Delta S°$
CBM-DK					
Laminarin	0.12	1.32 (±0.08)×10^6	−8.35	−112 (±2)	−103
Laminaritetraose	0.99	1.63 (±0.28)×10^4	−5.74	−11.2 (±3.6)	−5.46
Laminarihexaose	0.95	3.46 (±0.18)×10^4	−6.19	−11.9 (±0.7)	−5.71
D311A/D355A					
Laminarin	0.10	4.25 (±0.82)×10^5	−7.67	−89.1 (±8.2)	−81.4

The S.D. were based upon fitting errors

laminarin and laminarioligosaccharides through a hydrophobic interaction, as observed with the carbohydrate recognition by CBMs [15, 16]. In CBM13 of *Streptomyces lividans* xylanase 10A, hydrophobic ring stacking interactions are observed at conserved residues, Trp34 in the α-repeat, Tyr74 in the β-repeat, and Tyr117 in the γ-repeat [6]. Similar hydrophobic interactions are also observed in CBM13 of *Streptomyces olivaceoviridis* E-86 xylanase [7, 8]. The corresponding residues in CBM-DK are Val285, Trp326, and Trp371, respectively (Fig. 1a). In our experiments using the mutants V285A, W326A, and W371A, the strength in binding to laminarin was similar to that of CBM-DK wild-type (data not shown). In this CBM, Trp273 in the α-repeat could contribute to

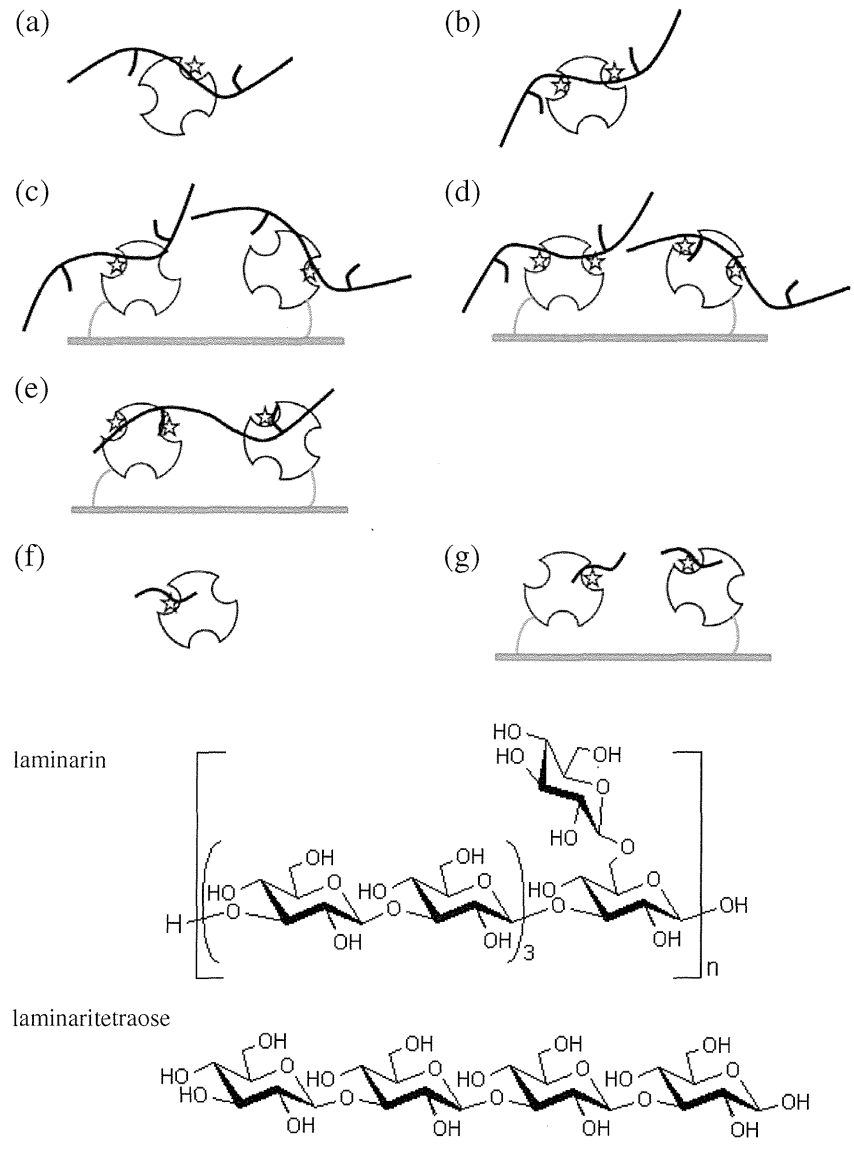

Fig. 5 Schematic representation of CBM-DK binding to laminarin and laminarioligosaccharide. **a** Monovalent binding to laminarin in solution. **b** Multivalent binding to laminarin within a single CBM-DK molecule in solution. **c** Monovalent binding to laminarin within a single CBM-DK molecule immobilized. **d** Multivalent binding to laminarin within a single CBM-DK molecule immobilized. **e** Multivalent binding to laminarin within multiple CBM-DK molecules immobilized. **f** Monovalent binding to laminarioligosaccharide in solution. **g** Monovalent binding to laminarioligosaccharide within a single CBM-DK molecule immobilized. The curved long bars with branches, curved short bars, and circles with hollows represent laminarins, laminarioligosaccharides, and CBM-DKs, respectively. The stars refer to the binding of CBM-DK to glucose unit of laminarin and laminarioligosaccharide. The chemical structures of laminarin and laminaritetraose are also indicated. The branched position of β-(1-6) linkage in laminarin is heterogeneous, and the ratio of β-(1-3) to β-(1-6) linkages is 7:1 [12]

CBM-DK binding of β-glucan. Because the residues corresponding to Trp273 in the β- and γ-repeats are Asp314 and Gly358, respectively, the additional binding effects would be much less than that of Trp273.

The ITC experiments showed that the binding stoichiometry for laminarioligosaccharides was approximately 1. Considering that the α-repeat primarily contributes to β-glucan binding, the laminarioligosaccharide would bind to the site on the α-repeat with the heat observed. Because the binding strength of laminarin to CBM-DK in solution is about 2-orders higher than those of laminarioligosaccharides, the β- and/or γ-repeats would be involved in the glucan binding. While laminarin is long enough to interact with multiple sites in the 2 or 3 repeats, laminarioligosaccharides are not (Fig. 5). In laminarin binding, the site on the α-repeat would first bind and localize it, and then other site(s) on the β- and/or γ-repeats could bind it in a cooperative manner, resulting in a binding strength to laminarin that is higher than those to laminarioligosaccharides. The binding stoichiometry for laminarin, 0.12, indicates that approximately 8 molecules of CBM-DK are involved in the complex formation with 1 molecule of laminarin. Assuming that the 8 CBM-DK molecules bind to laminarin independently, the binding enthalpy change (ΔH) derived from 1 CBM-DK molecule can be estimated to be approximately −14 kcal/mol. This is lower than those for the binding to laminarioligosaccharides (Table 2), which is expected to be due to the multivalent binding of laminarin to the β- and/or γ-repeats in addition to the α-repeat.

In our analysis to determine the role of CBM13 in the enzymatic function of the appended catalytic domains, we and others have shown that CBM13 contributes to the hydrolytic activity for insoluble carbohydrates such as curdlan and yeast-glucan, but not for soluble carbohydrates such as laminarin and laminarioligosaccharides [4, 17–19]. Assuming that the insoluble carbohydrates are in the aggregated form and long enough to simultaneously bind to both the catalytic domain and the CBM13 of an endo-1,3-β-glucanase molecule, the CBM13 could contribute to localization of the catalytic domain on condensed carbohydrates, which could accelerate hydrolysis. For efficient catalysis in general, the enzyme should rapidly bind and release the substrate. Considering that the catalytic domain of endo-1,3-β-glucanase from *Cellulosimicrobium cellulans* DK-1 itself has the ability to bind to the substrates with a K_a value around 10^6 M^{-1} [19], the binding affinities of CBM-DK for the substrates determined in this study seem to be quite reasonable. The full-length endo-1,3-β-glucanase could bind to insoluble glucans tightly via CBM and release the shorter glucans as products.

Acknowledgments The authors thank Mr. Takahiro Maruno of Osaka University and Prof. Yuji Kobayashi of Osaka University of Pharmaceutical Sciences for technical support and helpful discussion. This work was partly performed under the Joint Usage/Research Program of Medical Research Institute, Tokyo Medical and Dental University.

References

1. Boraston, A.B., Bolam, D.N., Gilbert, H.J., Davies, G.J.: Carbohydrate-binding modules: fine-tuning polysaccharide recognition. Biochem. J. **382**, 769–781 (2004)
2. Shoseyov, O., Shani, Z., Levy, I.: Carbohydrate binding modules: biochemical properties and novel applications. Microbiol. Mol. Biol. Rev. **70**, 283–295 (2006)
3. http://www.cazy.org/Carbohydrate-Binding-Modules.html
4. Ferrer, P.: Revisiting the *Cellulosimicrobium cellulans* yeast-lytic β-1,3-glucanases toolbox: a review. Microb. Cell Fact. **5**, 10 (2006)
5. Tanabe, Y., Pang, Z., Oda, M.: Cloning and sequencing of endo-1,3-β-glucanase from *Cellulosimicrobium cellulans*. J. Biol. Macromol. **8**, 60–63 (2008)
6. Notenboom, V., Boraston, A.B., Williams, S.J., Kilburn, D.G., Rose, D.R.: High-resolution crystal structures of the lectin-like xylan binding domain from *Streptomyces lividans* xylanase 10A with bound substrates reveal a novel mode of xylan binding. Biochemistry **41**, 4246–4254 (2002)
7. Fujimoto, Z., Kuno, A., Kaneko, S., Kobayashi, H., Kusakabe, I., Mizuno, H.: Crystal structures of the sugar complexes of *Streptomyces olivaceoviridis* E-86 xylanase: sugar binding structure of the family 13 carbohydrate binding module. J. Mol. Biol. **316**, 65–78 (2002)
8. Fujimoto, Z., Kaneko, S., Kuno, A., Kobayashi, H., Kusakabe, I., Mizuno, H.: Crystal structures of decorated xylooligosaccharides bound to a family 10 xylanase from *Streptomyces olivaceoviridis* E-86. J. Biol. Chem. **279**, 9606–9614 (2004)
9. Arnold, K., Bordoli, L., Kopp, J., Schwede, T.: The SWISS-MODEL Workspace: a web-based environment for protein structure homology modelling. Bioinformatics **22**, 195–201 (2006)
10. Boraston, A.B., Tomme, P., Amandoron, E.A., Kilburn, D.G.: A novel mechanism of xylan binding by a lectin-like module from *Streptomyces lividans* xylanase 10A. Biochem. J. **350**, 933–941 (2000)
11. Schärpf, M., Connelly, G.P., Lee, G.M., Boraston, A.B., Warren, R. A., McIntosh, L.P.: Site-specific characterization of the association of xylooligosaccharides with the CBM13 lectin-like xylan binding domain from *Streptomyces lividans* xylanase 10A by NMR spectroscopy. Biochemistry **41**, 4255–4263 (2002)
12. Tanaka, S., Aketagawa, J., Takahashi, S., Shibata, Y., Tsumuraya, Y., Hashimoto, Y.: Activation of a limulus coagulation factor G by (1→3)-β-D-glucans. Carbohydr. Res. **218**, 167–174 (1991)
13. Oda, M., Azuma, T.: Reevaluation of stoichiometry and affinity/avidity in interactions between anti-hapten antibodies and mono- or multi-valent antigens. Mol. Immunol. **37**, 1111–1122 (2000)
14. Ho, S.N., Hunt, H.D., Horton, R.M., Pullen, J.K., Pease, L.R.: Site-directed mutagenesis by overlap extension using the polymerase chain reaction. Gene **77**, 51–59 (1989)
15. Alahuhta, M., Xu, Q., Bomble, Y.J., Brunecky, R., Adney, W.S., Ding, S.Y., Himmel, M.E., Lunin, V.V.: The unique binding mode of cellulosomal CBM4 from *Clostridium thermocellum* cellobiohydrolase A. J. Mol. Biol. **402**, 374–387 (2010)
16. Schouppe, D., Rougé, P., Lasanajak, Y., Barre, A., Smith, D.F., Proost, P., Van Damme, E.J.: Mutational analysis of the carbohydrate binding activity of the tobacco lectin. Glycoconj. J. **27**, 613–623 (2010)

17. Salazar, O., Molitor, J., Lienqueo, M.E., Asenjo, J.A.: Overproduction, purification, and characterization of β-1,3-glucanase type II in *Escherichia coli*. Protein Expr. Purif. **23**, 219–225 (2001)
18. Li, N., Shi, P., Yang, P., Wang, Y., Luo, H., Bai, Y., Zhou, Z., Yao, B.: A xylanase with high pH stability from *Streptomyces* sp. S27 and its carbohydrate-binding module with/without linker-region-truncated versions. Appl. Microbiol. Biotechnol. **83**, 99–107 (2009)
19. Tanabe, Y., Oda, M.: Molecular characterization of endo-1,3-β-glucanase from *Cellulosimicrobium cellulans*: effects of carbohydrate-binding module on enzymatic function and stability. BBA - Proteins Proteomics **1814**, 1713–1719 (2011)

BIOCHEMISTRY
including biophysical chemistry & molecular biology

Article

pubs.acs.org/biochemistry

Effects of DNA Binding of the Zinc Finger and Linkers for Domain Fusion on the Catalytic Activity of Sequence-Specific Chimeric Recombinases Determined by a Facile Fluorescent System

Wataru Nomura,*[,†] Akemi Masuda,[†,‡] Kenji Ohba,[§] Arisa Urabe,[†] Nobutoshi Ito,[‡] Akihide Ryo,[∥] Naoki Yamamoto,[§] and Hirokazu Tamamura*[,†,‡]

[†]Institute of Biomaterials and Bioengineering, Tokyo Medical and Dental University, 2-3-10 Kandasurugadai, Chiyoda-ku, Tokyo 101-0062, Japan

[‡]Graduate School of Biomedical Science, Tokyo Medical and Dental University, 1-45 Yushima, Bunkyo-ku, Tokyo 113-8510, Japan

[§]Department of Microbiology, Yong Loo Lin School of Medicine, National University of Singapore, Singapore 117597, Singapore

[∥]Department of Microbiology and Molecular Biodefense Research, School of Medicine, Yokohama City University, 3-9 Fukuura, Kanazawa-ku, Yokohama 236-0004, Japan

Supporting Information

ABSTRACT: Artificial zinc finger proteins (ZFPs) consist of Cys_2-His_2-type modules composed of ~30 amino acids with a $\beta\beta\alpha$ structure that coordinates a zinc ion. ZFPs that recognize specific DNA target sequences can substitute for the binding domains of enzymes that act on DNA to create designer enzymes with programmable sequence specificity. The most studied of these engineered enzymes are zinc finger nucleases (ZFNs). ZFNs have been widely used to model organisms and are currently in human clinical trials with an aim of therapeutic gene editing. Difficulties with ZFNs arise from unpredictable mutations caused by nonhomologous end joining and off-target DNA cleavage and mutagenesis. A more recent strategy that aims to address the shortcomings of ZFNs involves zinc finger recombinases (ZFRs). A thorough understanding of ZFRs and methods for their modification promises powerful new tools for gene manipulation in model organisms as well as in gene therapy. In an effort to design efficient and specific ZFRs, the effects of the DNA binding affinity of the zinc finger domains and the linker sequence between ZFPs and recombinase catalytic domains have been assessed. A plasmid system containing ZFR target sites was constructed for evaluation of catalytic activities of ZFRs with variable linker lengths and numbers of zinc finger modules. Recombination efficiencies were evaluated by restriction enzyme analysis of isolated plasmids after reaction in *Escherichia coli* and changes in EGFP fluorescence in mammalian cells. The results provide information relevant to the design of ZFRs that will be useful for sequence-specific genome modification.

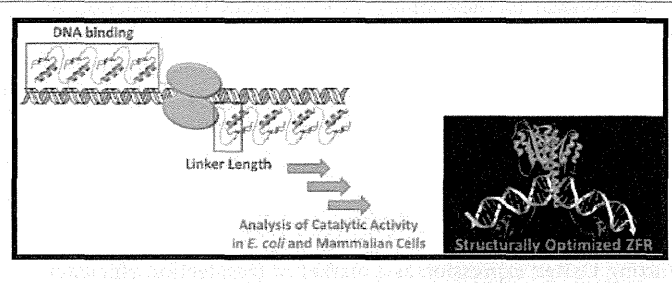

Artificial zinc finger proteins (ZFPs) can be used to engineer DNA binding domains with high specificity for desired target sequences, and ZFPs are a promising technology for gene therapy.[1−6] Modular assembly of ZFPs can create a DNA binding domain that targets virtually any sequence in the human genome.[3−5] By linking ZFPs to the catalytic domains of DNA-modifying enzymes, novel enzymes, including nucleases,[6] recombinases,[7−12] and methylases,[13−20] have been fabricated. These enzymes are endowed with programmable DNA binding specificity provided by the zinc finger protein fusion. Relevant to our development of ZFRs, recombinase enzymes from the serine recombinase family have been well studied.[21] In comparison with members of the tyrosine recombinase family such as Cre and Flp recombinases, the serine recombinases, including Tn3 and $\gamma\delta$ resolvases, Hin invertase, and Gin invertase, have DNA binding domains that are structurally independent of the catalytic domain. The structures of the catalytic domains and the sequences required for catalytic activity are highly conserved in these recombinases.[22] Tn3 and $\gamma\delta$ are among the best-characterized site-specific recombinase enzymes in the serine recombinase family. Only 35 amino acid residues differ between the $\gamma\delta$ and Tn3 resolvases, and their structures and functions are similar.[23] Negatively supercoiled DNA is a prerequisite for substrate recombination with native serine recombinase enzymes.[21] Although it is known that native serine recombinases require accessory proteins binding to sites I−III, activating mutants that require only the 28 bp of site I for successful recombination have been isolated.[7] In these hyperactivated enzymes, a DNA substrate in the form of negatively supercoiled DNA is not required for activity, and this allows application of activated catalytic domains with ZFPs to create zinc finger recombinases (ZFR). It has been suggested that reactions with serine recombinases proceed in three

Received: December 19, 2011
Revised: January 21, 2012
Published: January 23, 2012

   dx.doi.org/10.1021/bi201878x | *Biochemistry* 2012, 51, 1510−1517

steps: (i) formation of a dimer binding to the two forms of site I on the DNA, (ii) formation of a tetramer between the forms of site I, and (iii) strand exchange.[24,25] After the strand exchange reaction, the sequences between target sites are excised and the strands ligated (Figure 1).

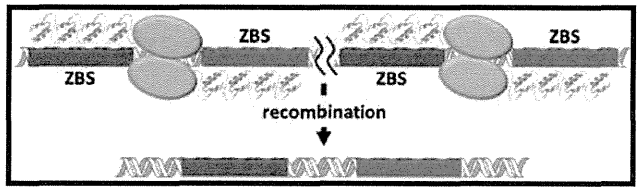

Figure 1. Schematic illustration of the ZFR reaction at a target site. The green and red boxes represent zinc finger binding sites (ZBSs). The yellow spheres represent catalytic domains of Tn3 resolvase.

ZFRs based on catalytic domain variants of Tn3, Gin, and Hin fused to artificial ZFPs have been shown to catalyze site-specific recombination in *Escherichia coli*[7−11] and mammalian cells.[8,9,11,12] ZFRs have also been shown to catalyze high-fidelity site-specific integration in mammalian cells.[9,11,12] While directed evolution of recombinase catalytic domains has proven to be essential for developing ZFR enzymes that function in mammalian cells, other aspects of ZFR design have not been thoroughly studied. In this report, we have synthesized ZFR mutants with variable numbers of zinc fingers and studied the role of peptide linkers that connect the Tn3 resolvase catalytic domain with the ZFP DNA binding domain. These effects are not readily addressed using molecular evolution strategies. For facile evaluation of recombination reactions in mammalian cells, a system that allows evaluation within 48 h was developed utilizing DsRed expression as a marker of transfection efficiency and EGFP expression as a marker of recombination efficiency. The results obtained revealed the optimal structures of the ZFRs, and the recombination efficiency results for linker mutants were verified by modeling studies.

EXPERIMENTAL PROCEDURES

Construction of ZFP Genes. ZFP genes were constructed as described previously.[26,27] Briefly, plasmid pc3XB encoding ZFPs purchased from Addgene (http://www.addgene.org) was repeatedly ligated. The zinc finger gene that was obtained was inserted into pMAL-p4x as an *Xba*I−*Bam*HI fragment for protein expression. A minor change was made to the multiple cloning site of pMAL-p4x (Figure S1 of the Supporting Information).

Target Enzyme-Linked Immunosorbent Assays (ELISAs). ELISA wells of 96-well plates were coated by incubation with 25 μL of 8 ng/mL streptavidin in PBS for 1 h at 37 °C. The plates were washed twice with dH_2O, and 25 μL of 5′-biotinylated hairpin oligonucleotide target in zinc buffer A (ZBA) [10 mM Tris-HCl (pH 7.5), 90 mM KCl, 1 mM $MgCl_2$, and 90 μM $ZnCl_2$] was added. After incubation for 1 h at 37 °C, plates were washed twice with dH_2O. Blocking solution (ZBA with 3% BSA, 175 μL) was added, and incubation continued for 1 h at 37 °C. The blocking solution was then removed; 25 μL of purified protein in ZBA was added, and 2-fold serial dilutions were performed into 1% BSA, 5 mM DTT, and 10 ng/μL salmon sperm DNA in ZBA. After incubation for 1 h at room temperature, the plates were washed 10 times with dH_2O and the monoclonal anti-MBP antibody (Sigma-Aldrich, 1:1000 dilution by ZBA with 1% BSA, 25 μL) was added. After incubation for 30 min at room temperature, the plates were washed 10 times with dH_2O and a diluted secondary anti-mouse IgG AP conjugate (Sigma-Aldrich, 1:1000 dilution by ZBA with 1% BSA, 25 μL) was added. After incubation for 30 min at room temperature, plates were washed 10 times with dH_2O. The alkaline phosphatase reaction was performed with *p*-nitrophenylphosphate for 30 min, and the absorbance at 405 nm was read with a microplate reader. The data were collected and plotted. The data were fit to the equation $y = 1/(1 + K_d/x)$, where y is the proportion of bound MBP−ZFP fusion protein to maximal binding derived from the absorbance at 405 nm and x is the concentration of the MBP−ZFP fusion protein. The K_d values are averages of three or more independent experiments, and standard errors of the mean (SEM) are shown.

Construction of ZFR Substrates. Each substrate plasmid contained a recombination cassette composed of two ZFR recombination sites flanking an EGFP gene as a stuffer sequence. Cassettes were assembled by amplifying the EGFP gene with primers encoding the ZFR site. The polymerase chain reaction (PCR) product was cloned into pAra-OP.[20] ZFP genes were amplified by PCR from plasmid pc3XB and inserted into the plasmid as *Eco*RI−*Sac*I fragments. Plasmids that contained ZFR with Gly-Ser linkers were mutated at the *Bst*BI site before insertion of the catalytic domain.

Construction of ZFR Genes. The DNA fragment of the Tn3 resolvase catalytic domain was amplified from pWL625 (ATCC accession number 31787) utilizing 5′-GAGGAG-GAATTCATGCGACTTTTTGGTTACGCT-3′ and 5′-GAG-GAGAAGCTTTCACGAGGCCCTTTCGTCTT-3′ as primers. The fragment was inserted into pBluescriptSK(−) as an *Eco*RI−*Hin*dIII fragment. Tn3-activating mutations (R2A, E56K, G101S, D102Y, M103I, and Q105L) were introduced into the Tn3 encoding gene. Linker sequences were amplified via PCR with the Tn3 fragment by primers that included the linker sequence. Tn3 fragments with different linkers were digested with *Eco*RI and *Bgl*II and ligated into similarly digested pAra-OP with the EGFP and ZFR sites. Tn3 fragments with various Gly-Ser linkers were also digested with *Eco*RI and *Bst*BI and then ligated. The plasmids were maintained with chloramphenicol.

Assay of Recombination of Plasmids in *E. coli*. The plasmid with a ZFR gene downstream from the arabinose promoter and the substrate sequences were introduced into *E. coli* by electroporation. After incubation for 14 h at 37 °C on an LB-agar plate, colonies were picked up and grown for 14 h at 37 °C in LB medium. Purified plasmids were digested with *Eco*RI for 1 h at 37 °C. After electrophoresis on a 0.8% agarose gel, the fragment intensity was estimated with ImageJ (Figure S2 of the Supporting Information).

Recombination Reaction of ZFR in Mammalian Cells. The EGFP gene, flanked by recombination sites, was inserted between *Nhe*I and *Kpn*I in pcDNA5/FRT (Life Technologies). A double-stranded oligonucleotide encoding the upstream target site was inserted into the *Mlu*I site, and the other oligonucleotide for the downstream target site was inserted into *Kpn*I and *Bam*HI sites. Cotransfection of the substrate plasmid and Flp expression plasmid (pOG44, Life Technologies) allowed site-specific integration into the single FLP recombinase target (FRT) site present in the Flp-In-CHO cell line (Life Technologies). Colony-acquired hygromycin resistance was characterized by fluorescently activated cell sorting (FACS) and genomic PCR. The sequence of the target site was confirmed. Cells were maintained in Ham's F-12 containing 10% (v/v)

dx.doi.org/10.1021/bi201878x | *Biochemistry* 2012, 51, 1510−1517

Table 1. DNA Binding Affinities of ZFPs

	two fingers	three fingers	four fingers	five fingers	six fingers
K_d (nM)[a]	160±20	23.6±3.6	12.8±1.1	15.4±1.4	12.9±1.4
R^2	0.90	0.87	0.94	0.94	0.94

[a]The values are averages of three or more independent experiments.

FBS and antibiotics (Wako Chemicals). The DsRed expression vector was constructed as follows; a DsRed-monomer sequence was ligated into pIRES2-EGFP (Clontech) to substitute for EGFP, and a Tn3-ZFP-NLS fragment was inserted between *Nhe*I and *Eco*RI in pIRES2-DsRed. On the following day, after 2 × 10^5 cells had been seeded, the ZFR expression vector was transfected into cells using Lipofectamine LTX Reagent and PLUS Reagent (Life Technologies). After being transfected for 48 h, cells were collected and analyzed by flow cytometry.

Molecular Modeling of the Linker Variants of ZFR. Computer models were generated using Discovery Studio (Accelrys Inc.). The crystal structure of the γδ resolvase–DNA complex [Protein Data Bank (PDB) entry 1GDT][22] was manually mutated in the protein and DNA to match the molecules used in this study. The first zinc finger module, obtained from a zinc finger–DNA complex (PDB entry 1MEY),[28] was placed on the resolvase–DNA complex by superimposing the phosphate backbone atoms of corresponding DNA residues. Appropriate linker atoms were then added and optimized by simulated annealing and energy minimization. During this optimization, the atoms in the resolvase, zinc fingers, and DNA were fixed, allowing only linker atoms to move.

RESULTS

Construction of Zinc Fingers and DNA Binding Analyses. The 18 bp target sequence of the zinc finger protein utilized in this study was 5′-CTGCATGCACTGGATGCA-3′.

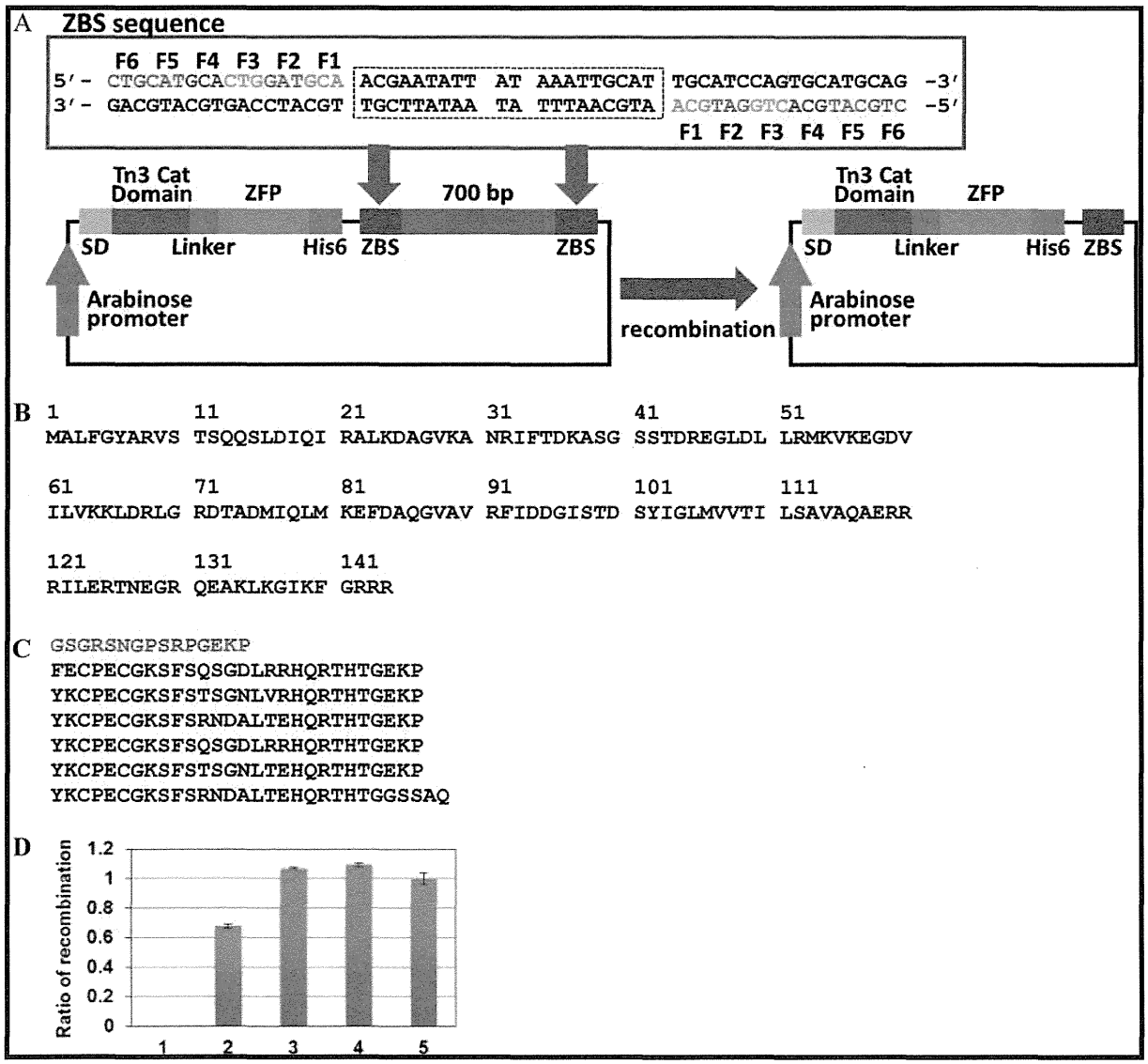

Figure 2. (A) Schematic of recombination at zinc finger binding sites (ZBSs). Recombination results in smaller plasmids. ZBS sequences are shown in the box. SD represents the Shine-Dalgarno sequence. (B) Amino acid sequences of the hyperactivated Tn3 catalytic domain. (C) Amino acid sequences of the linker (red) and six-zinc finger domain utilized for the analysis in *E. coli*. (D) Recombination efficiency depends on the number of fingers in ZFR. Columns 1–5 show the recombination efficiencies of two- through six-finger modules. The ratios are relative to the efficiency of the six-finger module. The error bars show the SEM of three or more independent experimental results.

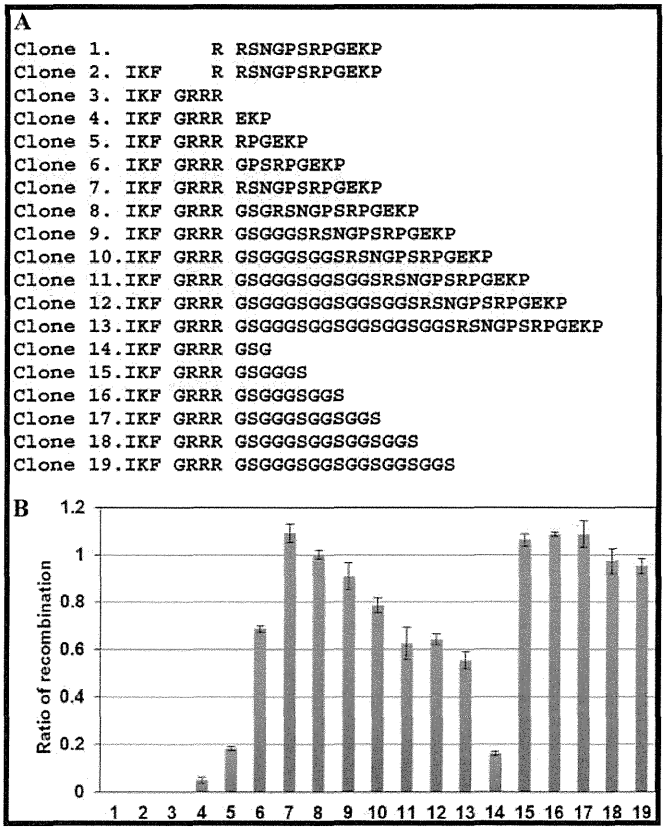

Figure 3. (A) Amino acid sequences of linkers of clones. All linkers were tested in the context of six-finger binding domains. (B) Results of recombination efficiency of clones with different linker sequences. The numbers of columns correspond to the clone numbers as described in panel A. The ratios are relative to the efficiency of clone 8. The error bars show the SEM of three or more independent experimental results.

Zinc fingers were constructed on the basis of a modular assembly strategy described by Barbas and co-workers.[27,29−32] Two- to six-finger proteins were constructed to obtain DNA binding domains with different affinities. Proteins were expressed as maltose binding protein fusions and purified with an MBPTrap column (GE Healthcare). The purity of the proteins was determined to be >90%. The DNA binding affinities were evaluated by an ELISA with the biotinylated hairpin oligonucleotide as a target.[10] The binding constants (K_d) of the two-, three-, four-, five-, and six-finger modules, listed in Table 1, were found to be 160, 23.6, 12.8, 15.4, and 12.9 nM, respectively. These results indicate that in the two-, three-, and four-finger modules, the DNA binding affinity increased with finger number but the binding affinities of ZFPs with four, five, and six fingers were similar.

Construction of ZFR Chimeric Proteins and Recombination Analysis in *E. coli*. The target DNA sequence of ZFR is shown in Figure 2A. The target site consists of a 20 bp spacer sequence flanked by 18 bp zinc finger binding sites. The spacer region was previously shown to be a Z+4 site in the target spacer of Z-resolvase.[7] For the evaluation of recombination in *E. coli*, a plasmid-based recombination system was constructed. The coding sequence of ZFRs was inserted into the plasmid containing a 700 bp stuffer sequence flanked with target sequences. In the recombination mediated by the expressed ZFRs, the stuffer sequence is excised to produce a smaller plasmid (Figure 2A). The amino acid sequences of the hyperactivated Tn3 catalytic domain, the linker between the domains, and the zinc finger domain are shown in panels B and C of Figure 2. The recombination efficiency was evaluated by a restriction enzyme assay. Plasmid purified from *E. coli* was digested by *Eco*RI, which is a single cutter of the plasmid. The linear plasmid was analyzed on an 0.8% agarose gel, and the fractions of the longer (nonrecombinant) and shorter (recombinant) plasmids were evaluated (Figure S2 of the Supporting Information). ZFR variants with different numbers of fingers were evaluated in this recombination system, and recombination ratios increased with increasing numbers of fingers from two to four fingers. The values of recombination efficiencies for ZFRs with four to six fingers were similar, reflecting the DNA binding affinities (Figure 2D). The production of recombinant sequence was confirmed by DNA sequencing analysis (Figure S3 of the Supporting Information).

In the next study, the reactions of ZFR variants with different linker lengths in the context of the six-finger module were tested (Figure 3B). In this experiment, 19 constructs were prepared. The variants were categorized into three groups depending on lengths and the compositions of linker sequences. The first group variants have short linkers with deletions within the catalytic

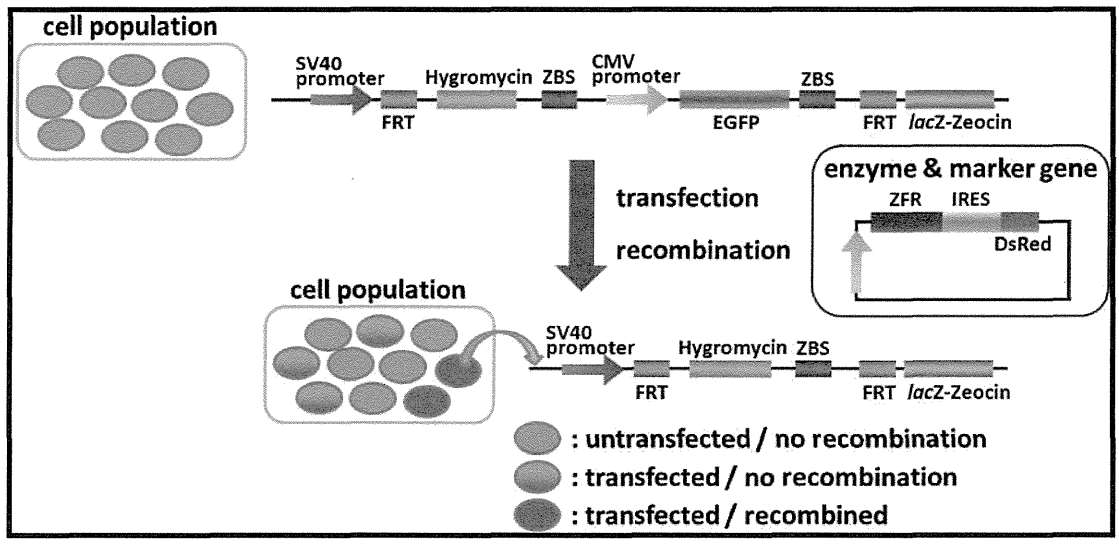

Figure 4. Recombination system constructed utilizing Flp-In-CHO-K1 cells.

domain of Tn3 resolvase (clones 1 and 2). The second group of variants has semirigid linkers (clones 3–13). The third group has flexible linker sequences composed of Gly-Ser sequences (clones 14–19). In the clones of the third group, the first two amino acids of the zinc finger domain, Tyr and Lys, are substituted with Phe and Glu, respectively. The recombination efficiencies were determined in the *E. coli*-based assay (Figure 3B). The results indicate two important phenomena. (1) The variant with a 12-amino acid linker was the most efficient (clone 7, Figure 3A), suggesting that there is an optimal linker length. (2) The variants with linkers composed of only Gly-Ser sequences were most efficient (clones 15–17, Figure 3A), indicating that ZFRs with flexible linkers tended to recombine most efficiently.

ZFR-Catalyzed Recombination in Mammalian Cells. To evaluate the recombination efficiency of ZFR variants in mammalian cells, we constructed a reporter cell line from Flp-In-CHO-K1 containing a cassette that encodes EGFP driven by a CMV promoter flanked by target sites (Figure 4). As each cell contains a single copy of the reporter gene, the recombination efficiency can be calculated from the proportion of cells with or without EGFP fluorescence. Additionally, the expression of ZFR was monitored by the expression of DsRed; this gene was placed downstream of the ZFR gene via a IRES sequence. The genes encoding ZFRs utilized in this study were amplified from a pAra plasmid shown in Figure 2A. Thus, the sequences of clones are the same as those utilized in experiments in *E. coli*.

With this reporter system, recombination efficiencies could be evaluated 48 h after transfection. Reported procedures involving retroviral-based transduction, selection, and evaluation take nearly 10 days.[8] The fluorescence intensity of cells was detected by FACS analysis (Figure S4 of the Supporting Information). The cells with recombinant genes were those that were EGFP-negative and DsRed-positive. The recombination efficiencies depended on the number of finger modules and on the linker lengths (Figure 5). As in *E. coli*, the five-finger proteins were the most efficient in recombination. The optimal linker length was six residues, which is different from that in *E. coli*. Additionally, recombination in mammalian cells was not as efficient as that in *E. coli*.

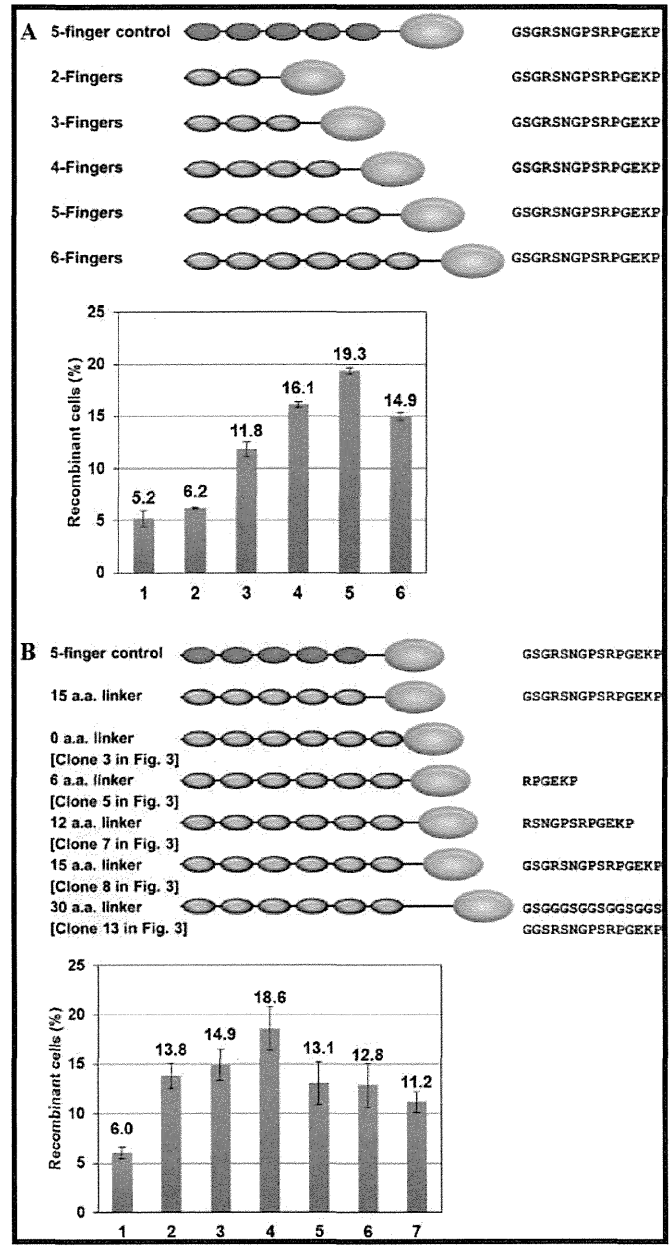

Figure 5. Recombination efficiency of ZFRs containing various numbers of fingers (A) and with various linkers (B) in mammalian cells. The top cartoons represent ZFR constructs utilized in the analyses. Green, blue, and yellow spheres represent zinc finger modules without sequence specificity, zinc finger modules with sequence specificity, and the Tn3 catalytic domain, respectively. Letters at the right of the cartoons are the linker sequences of the constructs. (A) Dependence on the number of fingers of ZFRs. The columns are as follows: column 1, five-finger control (nonspecific DNA binding); column 2, two fingers; column 3, three fingers; column 4, four fingers; column 5, five fingers; column 6, six fingers and different linker lengths. (B) Dependence on linker length. The columns are as follows: column 1, nontarget five-finger control with 15 amino acids; column 2, targeted five-finger ZFR with 15-amino acid linker; columns 3–7, targeted six-finger ZFRs with linker lengths of 0, 6, 12, 15, and 30 amino acids, respectively. The error bars show the SEM of three or more independent experimental results.

DISCUSSION

This study demonstrated that ZFR recombinases can be designed to specifically target sites in *E. coli* and mammalian cells and that recombination efficiency depends on the affinity of the ZFP for the DNA target and on the length of the linker between the DNA binding domain and the recombinase domain. The ZFR with five fingers had the highest recombination efficiency in both *E. coli* and CHO-K1 cells. The DNA binding affinity of this particular ZFP was saturated when the DNA binding domain had more than five fingers. The association and dissociation with DNA binding depend on the number of finger modules.[33] It is possible that the ZFR with five fingers was the most efficient recombination because the balance of association with dissociation and turnover was optimal. Guo et al. have also reported that four and five ZF domains are optimal for activity of ZFN.[34] On the basis of our data, the apparent K_d values of the four-, five-, and six-finger proteins derived from this particular ZFP were similar. The dependence on the number of finger modules was common in both *E. coli* and mammalian cells, but the recombination efficiency was lower in mammalian cells. In CHO-K1 cells, DNA is sequestered in chromatin structures. Additionally, the circular form of plasmid DNA could enhance recombination in the bacterial cells.

Recombination efficiency was dependent on the linker between the zinc finger domain and the recombinase domain. ZFRs with the shortest linkers had a very low efficiency of

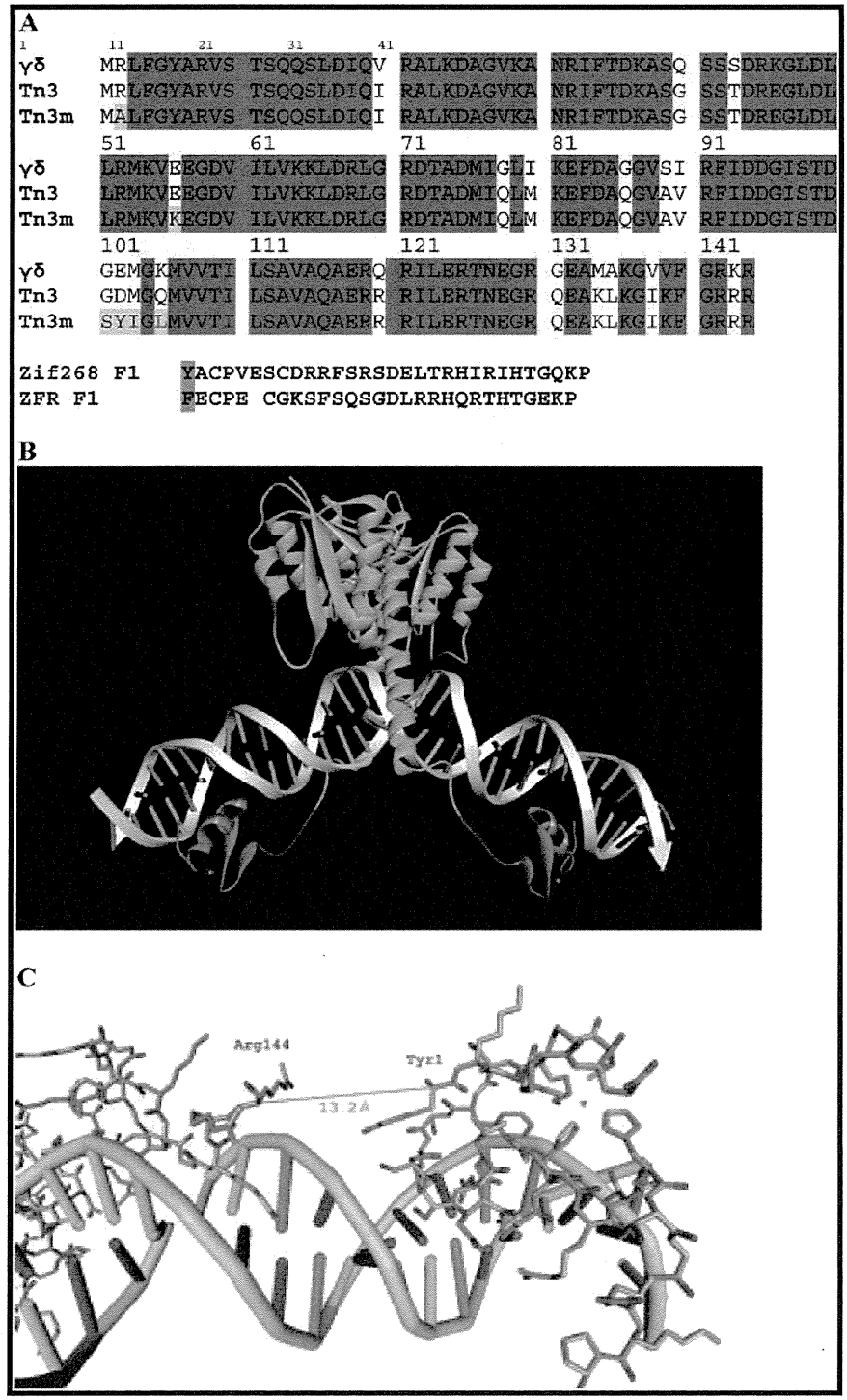

Figure 6. Representative result of molecular modeling of the resolvase domain and the first zinc finger module separated by a six-amino acid linker sequence. (A) Sequence alignment of resolvases $\gamma\delta$ and Tn3 and the Tn3 hyperactivated mutant (Tn3m) (top), the first finger of zif268, and ZFR. Conserved residues are highlighted in red, and amino acid substitutions in the hyperactive mutant are highlighted in yellow. The N-terminal aromatic amino acids of zinc fingers are highlighted in blue. (B) The yellow ribbon indicates $\gamma\delta$ resolvase, the red ribbon the six-amino acid linker, the green ribbon the N-terminal zinc finger domain, and the gray ribbon the zinc ion. (C) Distances between Cα atoms of Arg144 and tyrosine (Tyr) at the N-terminus of zif268. The N-terminal amino acid of the zinc finger domain is phenylalanine (Phe) in ZFRs utilized in this study.

recombination in both bacterial and mammalian cells. Second, the length of linkers based on the original sequences was critical. Proteins with linkers containing 12 amino acid residues were the most efficient in recombination. In the Gly-Ser linker variants, the recombination efficiency reached a maximum at six amino acids. This result indicates that both the length and the flexibility of the linker are important.

A molecular modeling study was performed in an attempt to assess the reasons for the differences in recombination efficiency among the linker mutants. In the modeling of the ZFR complex with target DNA, the linker length of six amino acids was optimal for the DNA binding of ZFR when the linker sequence was flexible (Figure 6A). When the domains were modeled bound to the target sequence, the distance between

dx.doi.org/10.1021/bi201878x | *Biochemistry* 2012, 51, 1510–1517